44th AIAA Aerospace Sciences Meeting and Exhibit
9 - 12 January 2006, Reno, Nevada

AIAA 2006-208

Simulation of Icing on a Cascade of Stator Blades

S. Lee [*], E. Loth[†], A. Broeren[‡] and M. Bragg[§]
University of Illinois at Urbana-Champaign, Urbana, IL, 61801

The effect of icing on turbo-machinery has been of recent interest due to certification requirements of engine operation and focus on optimum ice protection systems. In this project, we examine a STAGE 67A stator blade to represent a part of a turbo-machinery compressor stage. Numerical simulations use the Reynolds-Average Navier-Stokes (RANS) solver for the air flow coupled with Continuous Random Walk (CRW) for the droplet trajectory and impingement released upstream of stator blade. These results were coupled with LEWICE for ice formation on the stator blade. The overall methodology allows prediction of the impingement efficiency, the amount of ice formation, and the adverse effects on the aerodynamic performances. Changes in the flow field due to ice accretion can lead to boundary layer separations, which causes reduction in the flow turning angle and mass flow rate as well as increase in the total pressure loss. Icing accretion is significantly sensitive to droplet size, integration time, and temperature. However weak sensitivity was found with respect to turbulence and angle of attack.

I. Introduction

IN the past studies of ice accretion on aircraft aerodynamic surfaces have shown that icing can have serious performance and safety problems during the course of flight. Reports of aircraft crashes due to ice accretion have led to substantial experimental and computational investigation on this area of research. However, similar research in icing accretion on turbo-machinery is not as advanced though icing in the engine components can be a concern for engine manufacturers and ice protection system designers. There are a number of possible scenarios of the detrimental effects that can result from ice accretion. In an example of a turbo-fan engine, such would include icing on the fan outlet guiding vanes which can cause air flow blockage raising the fan operating line into stall, icing on booster inlet guide vanes that causes reduced flux of air and thus resulting slow fluid accelerations, and ice shedding that can damage the mechanical components down stream which later can cause stall and flameout of the engine.

In this study, the effect of ice accretion on the two-dimensional stator cascade in the compressor stage, which is an idealized form of the full three-dimensional condition, is investigated numerically. In particular, the first stator after the fan in the turbomachinery is simulated, since this is the part where most ice is accumulated. An outline of the numerical methodology for computing the flow field and ice accretion prediction will be discussed, followed by some validation of the numerical tools and the results for various flow conditions.

II. Computational Methodology

Three stages of numerical computation are employed to predict ice accretion and flow changes in the stator cascade as can be observed from Fig. 1. First, the Reynolds-Averaged Navier-Stokes (RANS) solver called WIND is used to compute the initial flow field in the cascade. The WIND software package supported by the National Project for Application-Oriented Research in Computational Fluid Dynamics Alliance is used as the flow solver and for pre- and post-processing. WIND is a structured, multi-zone, node-centered finite volume method solving the full compressible Reynolds-averaged Navier–Stokes equations with flexible turbulence models. In particular, k-Ω turbulence modeling is used for our particular study. 'Gridgen' is used to generate the grids for the cascade used by WIND. Second, using the steady state flow solution, droplet trajectories and impingement efficiency on the surface of the stator are obtained by DROP, a program, which uses the Continuous Random Walk model [1, 2]. Third, the impingement efficiency distribution and static pressure distribution from WIND are used in LEWICE, developed by

[*] Research Assistant, Aerospace Engineering, Urbana IL 61801, AIAA Student
[†] Professor, Aerospace Engineering, Urbana IL 61801, AIAA Associate Fellow
[‡] Research Scientist, Aerospace Engineering, Urbana IL 61801, AIAA Member
[§] Professor, Aerospace Engineering, Urbana IL 61801, AIAA Fellow

NASA Glenn Research Center, to predict the ice accretion on the surface of the stator blade. The ice accretion over a short period of time will change the cross-section geometry of the stator blade. Next, a new grid is generated for ice accreted geometry. Then, a new Reynolds-Averaged Navier-Stokes flow solution is obtained by WIND to characterize the aerodynamics of the iced stator blade.

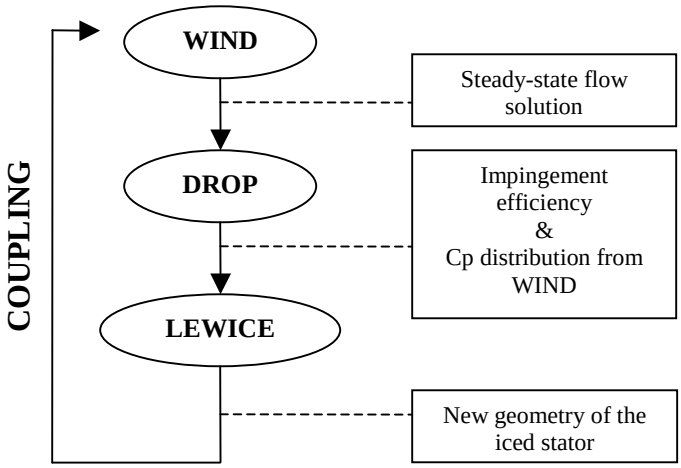

Figure 1. Schematic of the coupled ice accretion simulation technique

1. Stator Cascade

Since the first stage of the stator is simulated, the upstream condition for the stator cascade is uniform flow blowing at a fixed angle due to the rotating fan upstream (Fig. 2). A controlled-diffusion blade called Stage 67A [5] is used to obtain the flow field of the cascade. This is one of the most common blades used for research [6, 7, 8, 9] and is a replacement of the original double-circular-arc profiles of Stator 67. The Stage 67A blade not only has excellent peak adiabatic efficiency, but also has proven to sustain a wider rage of stall-free incidence than the double-circular-arc blades. This is because it is a controlled-diffusion blade which keeps the boundary layer thin and free of flow separation up to Mach 0.8 [8]. The flow solution herein is computed with WIND by using testing conditions in Table 1 in order to obtain a flow field similar to Sanger et al. [8, 9]. It is notable that the inlet Mach number is relatively low, but by increasing the chord length, a high chord Reynolds number is obtained, which is in the order of real-world chord Reynolds number for turbomachinery. Using the given testing conditions, a WIND flow solution is obtained, shown by the Mach number contours in Fig. 3a. The boundary layer is thin with almost no flow separation. Comparing the static pressure coefficient distribution (c_p) with the experimental data [8] in Fig. 3b, the flow field from WIND shows good agreement.

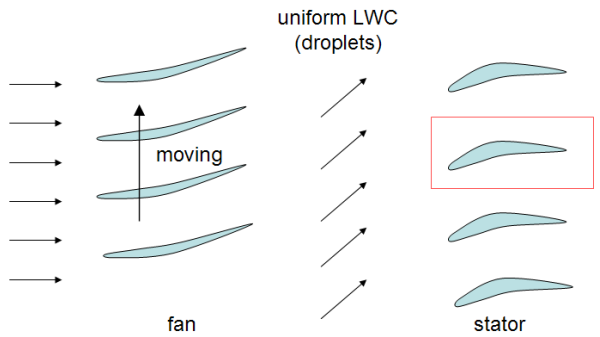

Figure 2. Uniform upstream flow

Table 1. Testing condition for stator cascade

Stage 67A CDC stator	Sanger et al. (1986) exper. cond.	Icing condition
Chord Length (C)	5.01 in	
Solidity (Chord/Pitch)	1.67	
Leading Edge Radius	0.0448 in	
Stagger Angle	14.4 deg	
Inlet Flow Angle	32.95 deg, 40.0 deg	
Speed	225 ft/s	200 ft/s
Altitude	Sea level	10,000ft
Temperature	65F	-22F ~ 30F
Chord Reynolds Number	583,000	461,000

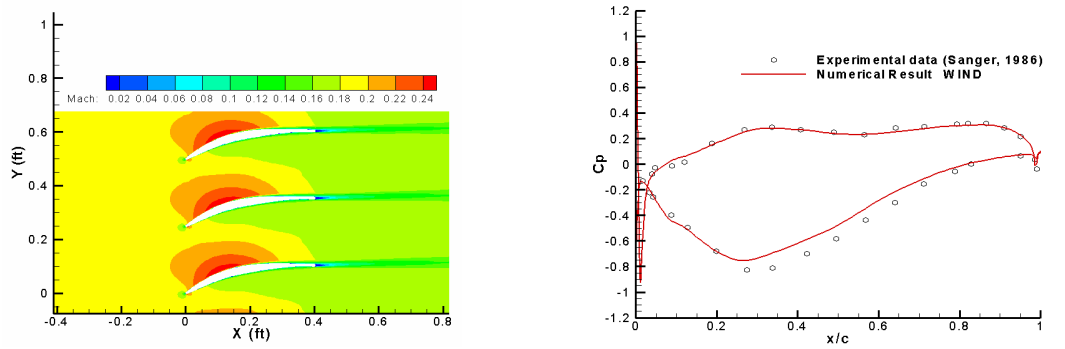

a) Mach contour and flow vectors **b) static pressure coefficient distribution**

Figure 3. Flow solution of Stage 67A stator cascade

2. Droplet Impingement Efficiency

The impingement efficiency distribution is obtained for droplets released uniformly upstream of an airfoil from DROP. As the droplet impinges on the airfoil surface two grid points on the airfoil surface over time (Fig. 4), the impingement efficiency β_i can be defined as the following

$$\beta_i = \frac{N_p / S_i}{N_{in} / S_{in}} \tag{1}$$

where, N_p is the number of droplets passing through the surface, S_i is the surface element area between two grid points, N_{in} is the total number of droplets released upstream through the surface, and S_{in} is the upstream total area for injection. The impingement efficiency β_i can be computed for each segment, or bin, over the wrapping distance of the airfoil to obtain an overall distribution. As droplets traverse across a panel S_i, an impingement is recorded for that panel. Each computational droplet trajectory is represented as a cloud of physical droplets with a Gaussian distribution in space. In particular, the impingement efficiency is computed using Gaussian Kernel Estimator [3] with a cloud variance of about 3/2 grid cells in size.

As a validation, impingement efficiency is compared with LEWICE and DROP with experimental data [4] shown in Fig. 5 for two droplet sizes. The numerical results from LEWICE and DROP agree relatively well with the experimental data. However, larger drops tend to have splashing effect which is not predicted with the current approach. Overall, these results indicate that DROP can be used as a valid tool to predict droplet impingement.

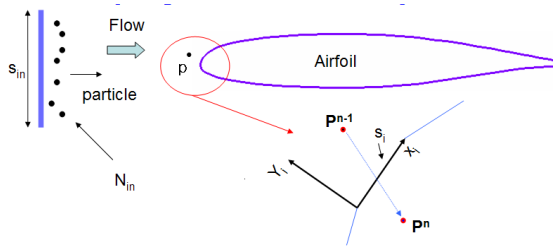

Figure 4. Illustration of impingement efficiency

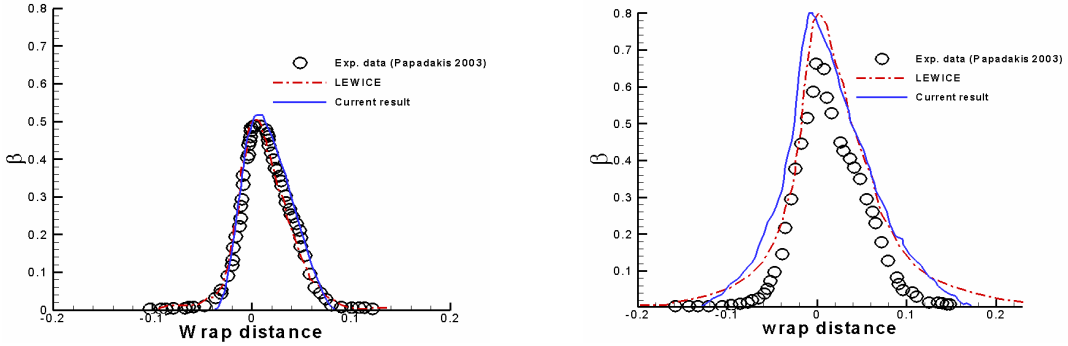

a) 21 µm droplet **b) 79µm droplet**

Figure 5. Impingement efficiency validation for MS317 airfoil

Using the flow field from WIND for Stage 67A stator cascade, DROP can be used to predict the impingement efficiency β for various droplet sizes. One aspect of typical compressor blade is that the modified inertia parameter, i.e. Stokes number, is typically much larger than that for airfoils for a given droplet size as a result of the decreased chord length (Table 1).

Table 2. Testing conditions for various droplets

Droplet diameter (μm)	Modified Inertia Parameter (Stokes Number)	
	MS317 Airfoil (36'' chord)	STAGE 67A Stator(5'' chord)
10	0.0037	0.025
20	0.040	0.287
79	0.31	2.33

Modified Inertia Parameter (Stokes number) is defined as

$$St_c = \frac{\tau_p}{\tau_c} \tag{2}$$

where, τ_c is the convective chord time scale and τ_p is droplet response time scale. Therefore, one may expect that droplet trajectories are less affected by the local streamlines for stator blades due to the higher inertial parameters. In addition, the leading edge of a stator blade is much sharper than that of a typical airfoil (Fig. 6a), which can also cause droplets to collect more at the leading edge for the stator case (as will be shown later).

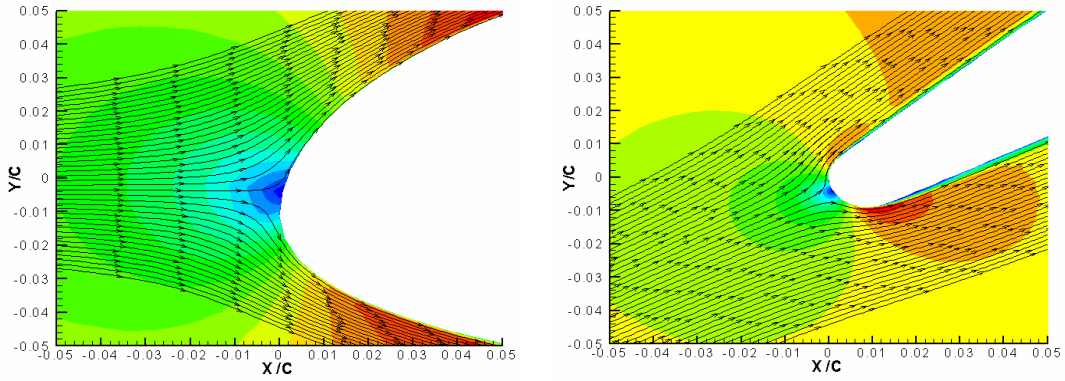

a) MS317 Airfoil **b) Stage 67A Stator**

Figure 6. Comparisons of streamlines zoomed at 5% chord

For a very large droplet, e.g. 1000 μm, the impingement efficiency should effectively equal the sine angle of the airfoil surface, for all the droplets released upstream impinge on the surface. Because of this, this condition can be used to help validate the DROP trajectories. Impingement efficiency for 1000 μm droplets (without gravity) is shown in Fig. 7a where there is very good agreement with the sine angle of the stator up to s/c=1.2. At further distances, there is a shadowing area where the droplets cannot reach on the top surface (Fig. 7b) so that the impingement efficiency given by DROP is zero.

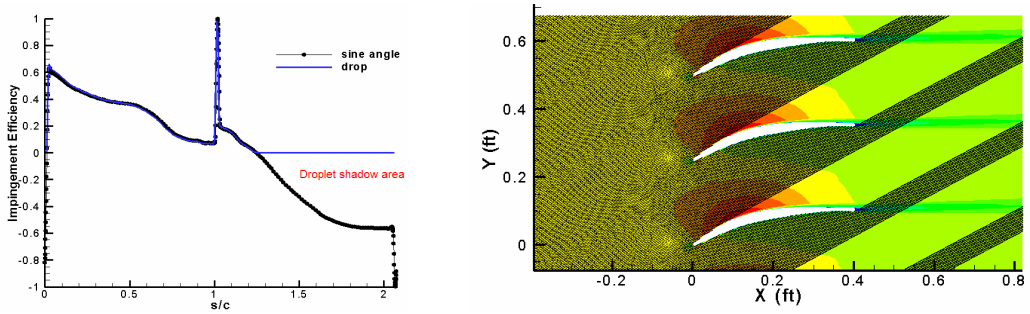

a) Stator sine angle and β **b) Droplet shadow area**

Figure 7. Validation of impingement efficiency for very large droplet

3. Ice Accretion Method

Using the above approach, one can simulate ice shape growth with and without coupling. The case without coupling was obtained for a 9-minute duration at 32.95° angle of attack with fixed c_p distribution and impingement efficiency from only the clean stator used for the LEWICE accretion (Fig. 8a). On the other hand, if we couple c_p distribution and impingement efficiency by updating them with each new geometry, differences can be expected, as shown in Fig. 8b, where the aerodynamic shape, c_p distribution and impingement efficiency distribution is updated for every 3minute icing encounter. Therefore, large ice accretion should be approached with a coupled method since intermediate accretions cause considerable deviations of the c_p distribution and impingement efficiency from the original values.

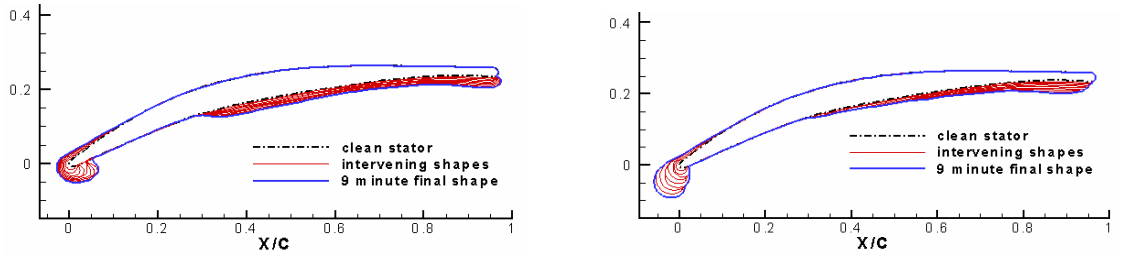

a) Uncoupled method **b) Coupled method**

Figure 8. Ice accretion method

III. Results

1. Ice Accretion on Stator

Various conditions were investigated to determine accretion and performance sensitivity to turbulence, integration time, droplet size, temperature and angle of attack. The first study considered the effects on impingement efficiency and ice accretion shape for droplet trajectories with and without turbulent diffusion included. This was studied for 5 μm size droplets released at 40.0° angle of attack at -4F static temperature condition. The results are shown in Fig. 9. Compared to the non-turbulent trajectory case, the turbulent impingement efficiency produce a lower leading edge peak and gave non-zero impingement on the pressure side of the stator (s/c from 0 to 0.5), as seen in Fig. 9a. This is due to the turbulent boundary layer where some of the droplets trajectories are driven by turbulent diffusion into the surface of the stator (whereas the non-turbulent case had a β of zero for s/c of 0 to 0.5). However the resulting ice-shape geometries are overall quite similar (Fig. 9b), though the turbulent case has somewhat smaller ice accretion at the leading edge. This is due to the lower peak value of the impingement efficiency at the leading edge compared with the non-turbulent case. As such, adding turbulence to the trajectories of

the droplet gave only a weak impact (especially for large droplet sizes), but was used for all remaining cases for consistency.

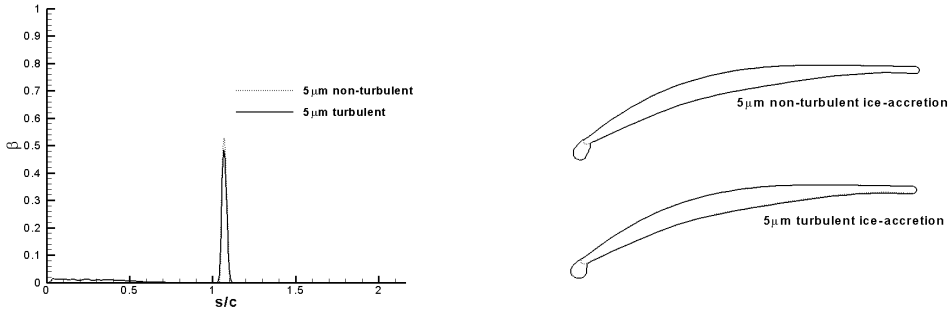

a) Impingement efficiency **b) Final iced geometry**

Figure 9. Impingement efficiency for turbulent and non-turbulent trajectories for 5μm droplets at -4°F and 40.0° AOA at 9 minute.

The next study examined ice time integrations of 3minute, 6 minute and 9 minute intervals for 79μm droplets released at 40.0° angle of attack at -4°F ambient temperature. The results are shown in Fig. 10 where it can be seen that the evolution is significant and non-linear in some places (the latter aspect is due to the coupling between the flow field and the ice accretion). Comparing Figs. 9 & 10 indicate that high peaks of the impingement efficiency at the leading edge due to large droplet sizes (higher Stokes number) causes the ice to grow larger along with a more downward direction. This downward growth is further enhanced by incoming droplets shadowing the region aft the leading edge. The variation due to droplet size is shown more clearly in Fig. 11 where large droplet size produce larger ice accretion. This is because smaller droplets have less inertia, thus are more likely to follow the flow and not impinge on the blade.

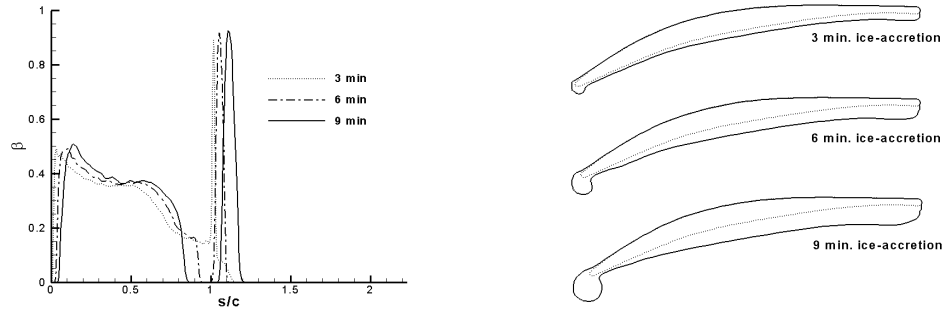

a) Impingement efficiency **b) Ice accretion at 3minute intervals**

Figure 10. Ice accretion growth with respect to time for 79μm droplet at -4°F and 40.0° AOA

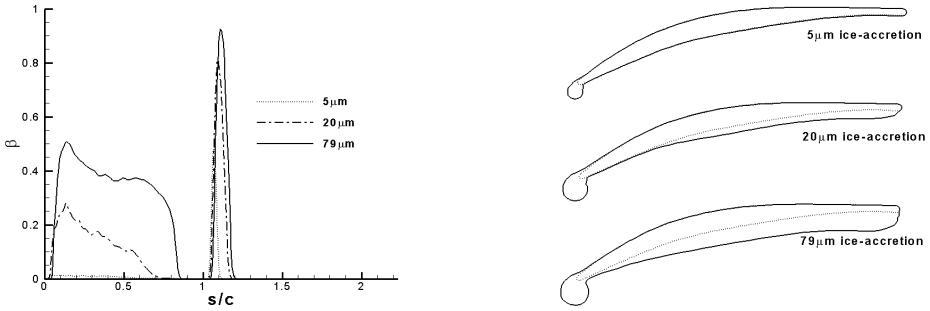

a) Impingement efficiency **b) Ice accretion for different droplet size**

Figure 11. Droplet size effect on the ice formation for -4°F and 40.0° AOA at 9 minutes

Temperature can also be important on ice accretion size and shapes as shown in Fig. 12. Ice formation is greatly reduced for temperatures near freezing (28°F), compared to the 12°F case, since the colder case has less melting. This is consistent with airfoil icing where by ice growth increases with lower temperatures for a fixed LWC. However, further decreases in temperature do not increase the ice size growth significantly because impingement efficiency and freezing reach a saturation point for the given drop size. In our numerical experiments, very similar ice shapes were produced for temperature ranging from 12°F to -22°F.

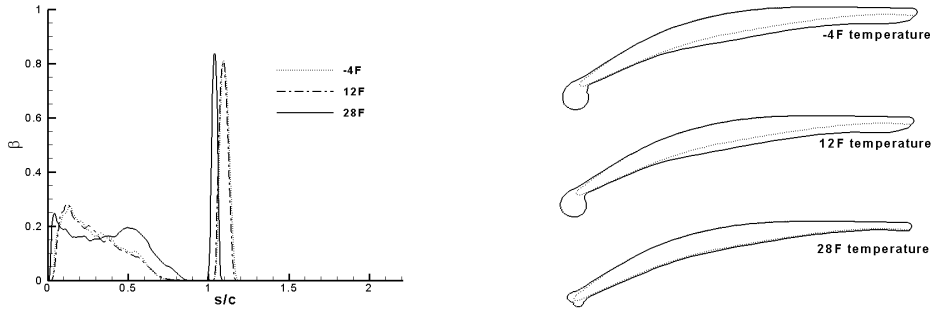

a) Impingement efficiency **b) Ice accretion for different temperature**

Figure 12. Comparison of ice formed at 9 minutes at different temperature is shown for 20μm droplets at 40.0° AOA

Lastly, the angle of attack effect on the stator ice accretion was investigated for two angles of attack (AOA); 32.95° and 40.0°, where the latter is the design angle of attack for the Stage 67A stator, where the former causes the pressure surface to be almost parallel with the upstream flow. The results are shown in Fig. 13, whereby the 32.95° case yields larger ice accretion at the leading edge but more rearward ice accretion on the pressure side surface aft the leading edge (due to camber). However, the differences are quite modest given the 7° angle change.

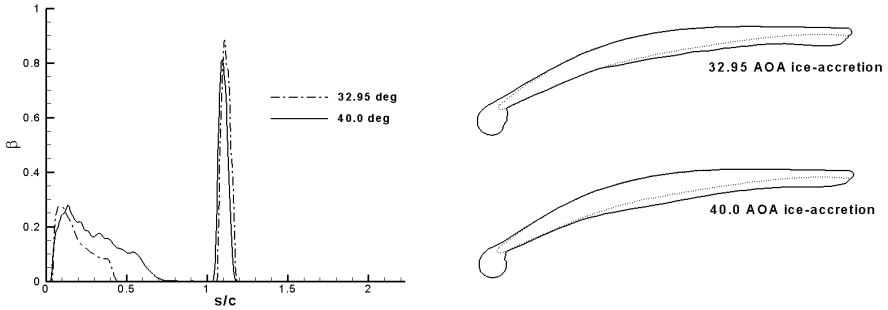

a) Impingement efficiency **b) Ice accretion for different angles**

Figure 13. Angle of attack effect on the 9 minute ice accretion for 32.95° and 40.0° for 20μm droplets at -4°F

2. Aero-performance

Based on the iced airfoil shapes examined above, aerodynamic changes due to ice accretions are investigated. Flow visualization of the leading edge and trailing edge flow fields are shown in Fig. 14 for clean and iced stators. In particular, Mach contours are plotted for the 32.95° angle of attack for clean stator and the 79μm droplet ice accreted stator. Large ice accretion at the leading edge causes major flow separation, whereas the clean stator shows almost no flow separation. Flow separation is detrimental as it can lead to stagnation pressure losses and mass flow rate losses through the cascade. Shown in Fig. 14c & d, the overall direction of the trailing edge streamlines for the clean stator is almost at zero degrees, whereas the streamline direction is upward for the iced stator case, indicating sub-optimal flow turning.

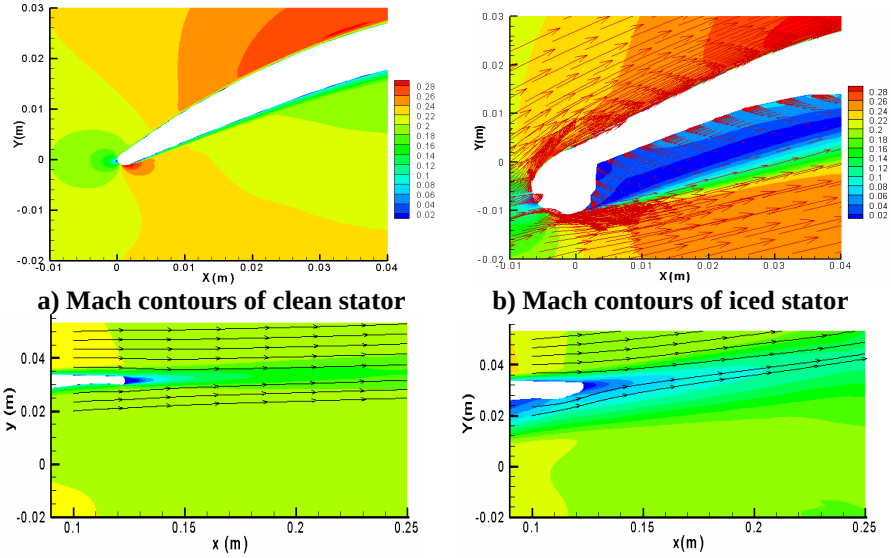

a) Mach contours of clean stator **b) Mach contours of iced stator**

c) streamlines for clean stator **d) streamlines for iced stator**

Figure 14. Mach contours and streamlines

To quantify the flow turning angle, along with total pressure loss and mass flow rate, three performance parameters are defined. An average flow turning angle ($\overline{\alpha}$) was computed based on integration of the local flow angles over the cascade exit. The dimensionless total pressure loss ($\overline{\omega}$) was computed by mass-averaging the stagnation pressure loss between the inflow and the cascade exit and normalizing this by the upstream dynamic head. Finally, the mass flow ratio ($\overline{m}$) was computed as the ratio of the mass flow through the cascade normalized by the mass flow rate of the clean case. The resulting performance parameters are shown in Tables 3 & 4. The clean cases at both 32.95° and 40.0° angle of attack yield an efficient stator flow which gives an average flow turning

Table 3. Aero-performance for 32.95° angle of attack

Case			$\overline{\alpha}$	$\overline{\omega}$	$\overline{m}$
AOA	diameter	Temp			
32.95	Clean	-4F	1.3	0.06	1.00
32.95	5μm	-4F	3.7	0.15	0.94
32.95	20μm	-4F	6.7	0.23	0.89
32.95	79μm	-4F	8.2	0.31	0.82
32.95	20μm	30F	2.5	0.10	0.93

Table 4. Aero-performance for 40.0° angle of attack

Case			$\overline{\alpha}$	$\overline{\omega}$	$\overline{m}$
AOA	diameter	Temp			
40.0	Clean	-4F	1.3	0.05	1.00
40.0	5μm	-4F	3.8	0.13	0.94
40.0	20μm	-4F	6.8	0.16	0.90
40.0	79μm	-4F	8.4	0.19	0.89
40.0	20μm	28F	3.0	0.12	0.96

angle close to zero and a low total pressure loss performance. For the iced stator cases, the flow turning angle and the non-dimensional total pressure loss was found to increase as the amount of accretion increased. This result was attributed primarily to leading edge flow separation. For the mass flow ratio, decreases were found to occur as accretion became more severe with values as low as 82%. However, it is interesting that the higher loaded 40.0^o angle of attack had better icing performance in terms of pressure loss and mass flow rate than the 32.95^o case.

IV. Conclusions

Simulation of icing on a cascade stator blades has been conducted to study the effect of ice accretion on the aerodynamic performance. Adverse effects due to ice accretion can lead to stall in the engine, which is detrimental to aircraft safety. In this study, an improved method of predicting ice accretion has been used, which is to couple the ice growth with c_p distribution and impingement efficiency distribution, enhancing the physical shape and size of the ice accretion. High peaks of impingement efficiency at the leading edge are due to large Stokes number, which does not allow the droplet to navigate around the leading edge. Such high peaks produced large ice accretion at the nose of the stator, which resulted in major flow separation, especially for large droplet sizes and low temperatures. Such flow separation increased the total pressure loss of the stator and also caused reduced flow turning angle, which can be detrimental to the performance of rotors and stators downstream. Furthermore, reduced mass flow rate caused by ice accretion indicates significant flow blockage effects.

Acknowledgments

We would like to acknowledge the support from Ohio Space Institute and technical input from General Electric, BF Goodrich and the NASA Glenn Research Center. The computations were performed with the support from National Center for Supercomputing Applications and UIUC Copper Linux Cluster Systems.

References

1 Bocksell, T. and E. Loth, "Discontinuous and Continuous Random Walk Models for Particle Diffusion in Free-Shear Flows," AIAA J. Vol. 39, No. 6, pp. 1086-1096, June 2001

2 Bhargava, C. E. Loth, and M. Potapczuk, "Numerical simulation of Icing Clouds in the NASA Glenn Icing Research Tunnel," AIAA Aerospace Sciences Meeting, AIAA-2004-0563

3 Silverman, B.W., "Density Estimation for Statistics and Data Analysis," Chapman & Hall, London, 1986

4 Papadakis, M., Rachman, A., Wong, S., "An Experimental Investigation of SLD Impingement on Airfoils and Simulated Ice Shapes," SAE International, 2003-01-2129, 2003

5 Sanger, N. L., "*The Use of Optimization Techniques to Design Controlled-DiffusionCompressor Blading*," Journal of Engineering for Power, Vol. 105, pp. 256-264,1983.

6 Hobbs, D. E., and Weingold, H. D., "*Development of Controlled Diffusion Airfoils for Multistage Compressor Application*," Journal of Engineering for Gas Turbines and Power, Vol. 106, pp. 271-278, 1984.

7 Dunker, R., Rechter, H., Starken, H., and Weyer, H., "*Redesign and Performance Analysis of a Transonic Axial Compressor Stator and Equivalent Plane Cascades with Subsonic Controlled Diffusion Blades*," Journal of Engineering for Gas Turbines and Power, Vol. 106, pp. 279-287, 1984.

8 Sanger, N.L., and Shreeve, R. P., "*Comparison of Calculated and Experimental Cascade Performance for Controlled-Diffusion Compressor Stator Blading*," Journal of Turbomachinery, Vol. 108, pp. 42-50, 1986.

9 Shreeve, R. P., Elazar, Y., Dreon, J. W., and Baydar, A., "*Wake Measurements and Loss Evaluation in a Controlled Diffusion Compressor Cascade*," Journal of Turbomachinery, Vol. 113, pp. 591-599, 1991.